Check for updates

Environmental Science Advances



Accepted Manuscript

This article can be cited before page numbers have been issued, to do this please use: J. Ying, L. Huang, S. Yu, S. Liu, Z. Wang, J. Chen and Y. Lu, *Environ. Sci.: Adv.*, 2025, DOI: 10.1039/D5VA00207A.



This is an Accepted Manuscript, which has been through the Royal Society of Chemistry peer review process and has been accepted for publication.

Accepted Manuscripts are published online shortly after acceptance, before technical editing, formatting and proof reading. Using this free service, authors can make their results available to the community, in citable form, before we publish the edited article. We will replace this Accepted Manuscript with the edited and formatted Advance Article as soon as it is available.

You can find more information about Accepted Manuscripts in the <u>Information for Authors</u>.

Please note that technical editing may introduce minor changes to the text and/or graphics, which may alter content. The journal's standard <u>Terms & Conditions</u> and the <u>Ethical guidelines</u> still apply. In no event shall the Royal Society of Chemistry be held responsible for any errors or omissions in this Accepted Manuscript or any consequences arising from the use of any information it contains.



View Article Online DOI: 10.1039/D5VA00207A

Environmental Significance Statement

The removal of organic compounds in industrial wastewater, due to their toxicity to both biological systems and the environment, has long been a challenging task. Photocatalysis, with its advantages of high efficiency and environmental friendliness, has been extensively investigated and applied in wastewater treatment. In this study, we developed a uranyl ion-loaded graphene oxide membrane via a simple one-step impregnation method, which is easy to recover and reuse while exhibiting photocatalytic degradation performance. Furthermore, the membrane demonstrates photocatalytic degradation capability towards tributyl phosphate (TBP), a common organic pollutant in nuclear industry wastewater. This work presents a strategy for utilizing uranyl ions in photocatalytic degradation of TBP, aligning with the "treat waste with waste" approach, and expands the application scenarios of heterogeneous photocatalysis involving uranyl ions.

ces Accepted Manuscrip

View Article Online DOI: 10.1039/D5VA00207A

ARTICLE

Uranyl-graphene oxide composite membrane for enhanced photocatalytic tributyl phosphate degradation

Jiahui Ying^{a,b}, Liqin Huang^a, Shanshan Yu^a, Shuang Liu^c, Zhe Wang^{a*}, Jing Chen^{a*}, Yuexiang Lu^{a*}

Received 00th January 20xx. Accepted 00th January 20xx

DOI: 10.1039/x0xx000000x

Tributyl phosphate (TBP), a common reagent in the PUREX spent fuel reprocessing, represents a significant organic pollutant and a challenging degradation target. This study leverages the inherent photocatalytic properties of uranyl ions (UO22+) for the treatment of radioactive organic waste. A uranyl-graphene oxide (U@GO) composite membrane is facilely fabricated via a one-step impregnation method. Comprehensive characterizations confirmed uranyl adsorption onto GO, inducing structural and chemical modifications. Systematic photocatalytic evaluation through rhodamine B degradation revealed significantly enhanced performance of U@GO membrane compared to free-state uranyl ions. Application of the composite membrane to TBP degradation demonstrated excellent photocatalytic efficiency, highlighted the potential of U@GO membrane for radioactive wastewater treatment. Combined with Electron Spin Resonance and Nuclear Magnetic Resonance characterizations, mechanistic investigation identified that the uranyl ions coordinated to GO membrane act as the primary active sites for photocatalysis. Upon light irradiation, the generated reactive oxygen species as well as the excited uranyl ions attacks TBP to degrade it to small, harmless molecules such as CO₂ and phosphoric acid, achieving complete mineralization. This work presents a novel approach for utilizing depleted uranium in catalytic applications and offers a promising new method and material for the efficient degradation of TBP.

1. Introduction

Depleted uranium, a by-product of nuclear fuel enrichment processes, is predominantly stockpiled as strategic reserves. While historically utilized for military purposes, recent scientific investigations have increasingly explored its potential in civilian applications. Catalysis has emerged as a frontier research domain within uranium chemistry, particularly focusing on uranyl ions (UO22+) - the predominant aqueous uranium species. These ions exhibit ligand-to-metal charge transfer (LMCT) under visible light irradiation, generating electronically excited states that undergo quenching through two primary pathways: single electron transfer (SET) with organic substrates or hydrogen atom transfer (HAT) from small molecules. Photoactivated uranyl complexes demonstrate remarkable catalytic versatility, enabling biomolecular cleavage, C-H bond functionalization, pollutant degradation, and photocatalytic hydrogen production. as well as the degradation of plastics (e.g., PVC, PET) and lignin, which have recently attracted significant attention¹⁻¹⁵. Some excellent reviews further detail uranium complex applications in organic synthesis and small molecule activation 16-18.

TBP, a key extractant in nuclear fuel reprocessing via the Purex process, demonstrates notable resistance to chemical degradation. During spent fuel treatment, nitric acid and irradiation generate degradation byproducts such as dibutyl phosphate (DBP), monobutyl phosphate (MBP), and butanol^{27,28}. Beyond nuclear applications, TBP serves critical roles in aerospace systems²⁹, textile manufacturing, and rare earth extraction processes. However, its effective removal remains a persistent challenge across industrial sectors. Reported degradation strategies include hydrolysis³⁰, wet-oxidation³¹, and biological processes³². Notably, photocatalytic processes have demonstrated effectiveness in degrading of TBP33,34.

Graphene oxide and its derivatives have emerged as prominent carbon-based nanomaterials in contemporary research. Characterized by their exceptional specific surface area, abundant surface functional groups, efficient photogenerated electron acceptor capabilities, and versatile solution processability, these materials demonstrate significant potential for enhancing photocatalytic performance through composite formation with various inorganic materials (e.g., ZnO ¹⁹, TiO₂²⁰, Fe₃O₄²¹). While uranyl ions have been successfully incorporated into diverse matrices including zeolites 22, clay23, mesoporous silicon²⁴, TiO₂²⁵, and other material. In our previous work, we synthesized highly adsorptive SiO₂ and verified its application in photocatalytic degradation after adsorbing uranyl ions²⁶. However, no studies to date have explored GO-uranyl composites for photocatalytic applications. This research gap primarily stems from the predominant focus on investigating adsorption capacity of GO for uranyl species rather than its photocatalytic synergies.

^{a.} Institute of Nuclear and New Energy Technology, Tsinghua University,

^{b.} Department of engineering physics, Tsinghua University, Beijing, 100084, P. R.

^{c.} Nuclear Research Institute for Future Technology and Policy, Seoul National University, Seoul 08826, Republic of Korea

Environmental Science: Advances

Currently, there is a scarcity of research into the photocatalytic degradation of TBP.

The application of uranyl is primarily limited by legal restrictions and radioactive concerns, making photocatalytic degradation of TBP in spent fuel reprocessing wastewater a feasible scenario. In this study, a simple one-step impregnation method is used to adsorb uranyl ions into graphene oxide, which is subsequently integrated into a membrane. The primary aim is to investigate the photocatalytic properties of the uranyl-adsorbed graphene oxide. Various characterization techniques are employed to compare the results with previous studies on the adsorption of uranyl by graphene oxide. Furthermore, the enhanced photoactivity of uranyl ions post incorporation of graphene oxide is verified using RhB. Finally, the composite membrane demonstrates its capability in photocatalytic TBP degradation, validating its practical applicability.

2. Materials and methods

2.1. Materials

This article is licensed under a Creative Commons Attribution-NonCommercial 3.0 Unported Licence

Open Access Article. Published on 12 November 2025. Downloaded on 11/18/2025 1:42:19 AM

 $UO_2(NO_3)_2 \cdot 6H_2O$ was obtained from the inventory of Institute of Nuclear and New Energy Technology, Tsinghua University. NaOH and HNO₃ were purchased from Aladdin. RhB was procured from Hebei Bailingwei Hyperfine Materials Co., LTD., while TBP was acquired from Beijing Tongguang Reagent. 0.22 μ m acetate fibre films were purchased from Shanghai Xingya Reagent Factory. All reagents used were analytically pure and required no further purification steps. The water employed in this study is 18.2 M Ω ultra-pure water sourced from Merck Milli-Q interal5 system.

2.2. Fabrication of photocatalytic composite membranes

The synthesis of graphene oxide utilized in this experiment was prepared as mentioned in our previous work³⁵. Synthesized graphene oxide was dispersed in an aqueous solution using ultrasonication and then diluted to a concentration of 0.12 g/L. Uranyl nitrate solutions were prepared at different concentration gradients (0-1000 ppm). The pH of the uranyl nitrate solution was adjusted to 5 using NaOH and HNO3, without affecting the concentration of uranyl ions. A mixture containing 5 mL of graphene oxide and 25 mL of uranyl nitrate solution was transferred into a centrifuge tube. After thorough mixing by oscillation, the mixture was further dispersed uniformly through ultrasonic treatment for 15 min, followed by continuous shaking at room temperature for 24 h on a shaker table. Subsequently, the resulting composite materials were extracted and filtered onto acetate fiber membrane substrates using a vacuum filtration device to form membranes, which were labeled as U@GO-X (X represents the initial uranyl nitrate concentration in ppm). Graphene oxide films that did not contain any uranyl ions were labeled as GO.

2.3. Photocatalytic measurement

2.3.1. RhB degradation experiment

Prepare a 10 ppm RhB solution and utilize 50, ml for each photocatalysis experiment. Adjust the pHPto \$048776 PNXOH2A7d HNO₃, ensuring no impact on the original RhB concentration. The CEAULIGHT CEL-HXF300-T3 light source system (visible light ,100 mW⋅cm⁻²) was employed as the xenon lamp source. All photocatalytic experiments were conducted under a circulating cooling water system at 298 K. The membranes were introduced into the RhB solution, followed by a dark reaction time of 4h to achieve complete adsorption before light ultraviolet irradiation commenced. The UV-5200 spectrophotometer from Shanghai Yuan Analysis Instrument was used to measure absorbance by sampling 2 mL every hour. In the TBP photocatalytic degradation experiment, a TBP concentration of 15 ppm with a solution volume of 100 mL and pH adjusted to 5. GC-MS analysis was performed for measuring TBP concentration.

2.3.2. Two-cup experiment and scavenging experiments

The two-cup experiment was performed as follows: Initially, U@GO-1000 and regular GO membranes were prepared through extraction and filtration processes. As per previous research conducted by our group, the film underwent reduction at 413 K for 4 hours to ensure complete blocking of uranyl ions and RhB molecules. Subsequently, the setup was assembled in the specified sequence with 100 mL of RhB solution and ultrapure water (pH=5) added separately into each cup. First, position U@GO-1000 towards the RhB solution and record the results of photocatalytic degradation. Then, switch the positions of the solution, that is, make GO face towards the RhB and record the results. Following a dark reaction period of 4 hours, light irradiation commenced and changes in absorbance within the solutions were recorded. In the scavenging experiments, the scavengers were used at a concentration of 5 mmol·L⁻¹.

2.4. Characterization

2.4.1. Instruments and Characterization

The U@GO-1000 material was utilized for characterization in the experiment. X-ray Diffraction (XRD) patterns were recorded on a Rigaku Ultima IV X-ray diffractometer with Cu Ka radiation (60 kV). Thermo Escalab250XiLUS X-ray photoelectron spectroscopy, was used for measuring the X-ray photoelectron spectrum (XPS), The binding energy was calibrated using C 1s photoelectron peak at 284.6 eV as a reference. Fourier transform infrared spectroscopy (FT-IR) was measured by ThermoFisher Scientific Nicolet iZ10 Fourier-transform infrared spectroscopy, with a scanning range of 500 cm⁻¹ to 4000 cm⁻¹. Using ZEISS GeminiSEM 360 scanning electron microscopy and Oxford AztecOne energy-dispersive X-ray spectroscopy (EDS) to observe the microstructure of the photocatalytic membrane and analyze the surface elements. The wavelength of the laser light source of Horiba Xplora Plus Raman spectroscopy is 532 nm, and the scanning range is from cm⁻¹ to 2000 cm⁻¹. Solid ultraviolet spectroscopy was tested by Shimadzu Company of Japan's UV3600IP UV-visible

Journal Name ARTICLE

spectrophotometry, with a test range of 200 nm to 800 nm. Additionally, photoluminescence (PL) spectra were acquired using Edinburgh Company's LP980 system, GO and U@GO-1000 were respectively dispersed in aqueous solution and tested at wavelengths ranging from 400 nm to 800 nm. The electron spin resonance (ESR) spectra were record using an X-band EPR spectrometer (JEOL, JES FA-200). The operating parameters were as following: microwave power = 1.0 mW; central magnetic field = 336 mT; sweep width = ± 5 mT; sweep time 100 s; modulation frequency = 100.00 kHz; and time constant = 0.03 s. ICP-MS analysis using Agilent 8900 ICP-MS triple Quad method was used to ascertain the loading capacity of the composite membrane. Using D₂O as the solvent, the ³¹P nuclear magnetic resonance (NMR) spectrum was recorded on a QOne Instrument Quantum-I Plus (400 MHz)

2.4.2. Measurement of TBP

This article is licensed under a Creative Commons Attribution-NonCommercial 3.0 Unported Licence

Open Access Article. Published on 12 November 2025. Downloaded on 11/18/2025 1:42:19 AM.

The GC-MS process is described as follows: The QP2010 analytical instrument manufactured by Shimadzu, Japan was utilized, and the capillary column employed was an Agilent HP-5 capillary column (30 m×0.25 mm i.d., 0.25 μm film thickness). Helium gas with a purity of 99.9999% was used as the carrier gas for column flow at a rate of 0.93 mL·min⁻¹. A sample volume of 1 μ L was injected into the GC system using an autosampler operating at 563 K in split mode with a ratio of 1/30. Initially, the oven temperature was set to 50 K and held for 3 min, followed by a temperature ramp of 20 K·min⁻¹ up to 543 K, resulting in a total run time of 14 minutes. The transfer line and ion source temperatures are maintained at 523 K throughout the analysis. MS detection operated in electron impact (EI) mode with an energy level of 70 eV. Confirmation of the target peak relied on both retention time and characteristic ion presence assessment. For quantitative testing purposes, selective ion monitoring (SIM) mode utilizing fragment ions at m/z values of both 99 and 155 was performed.

3. Results and discussion

View Article Online DOI: 10.1039/D5VA00207A

3.1. Characterization of composite membranes

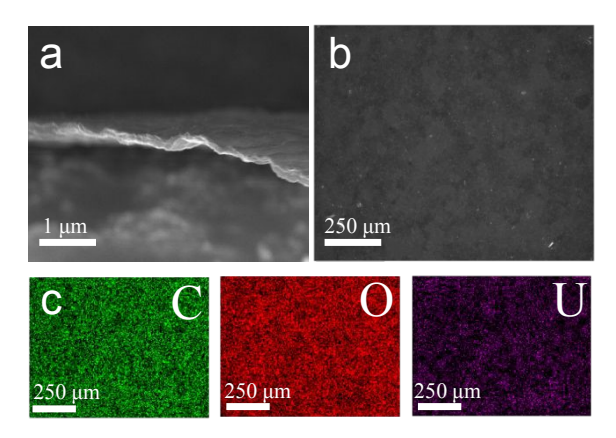


Fig. 1 SEM images of U@GO-1000 (a) The image of U@GO-1000 taken from the side (b) The image of U@GO-1000 taken from the front side (c) The energy-dispersive X-ray (EDX) elemental mapping; colour scheme: green for C; red for O; and purple for U.

In order to perform morphology characterization of the material, SEM and EDX are initially employed to observe the surface of U@GO-1000, as depicted in Fig. 1. From the side view presented in Fig. 1a, it can be observed that even after being pumped and filtered on the acetate fibre membrane, the material still exhibits a membranous structure with a thickness ranging from 100-200 nm. Contrary to typical graphene oxide membranes characterized by smooth and wrinkled surfaces, a rough yet uniform surface is observed in the front-facing image shown in Fig. 1b. The EDX element analysis displayed in Fig. 1c reveals an even distribution of uranium throughout the extracted membrane. These SEM results provide preliminary evidence indicating that upon adsorption of uranyl onto graphene oxide, the original layered lamellar structure is no longer present and is instead replaced by a lumpy structure. For a more accurate depiction of the process of uranyl ion adsorption on graphene oxide, we perform XRD, FT-IR spectrum,

View Article Online DOI: 10.1039/D5VA00207A

ARTICLE

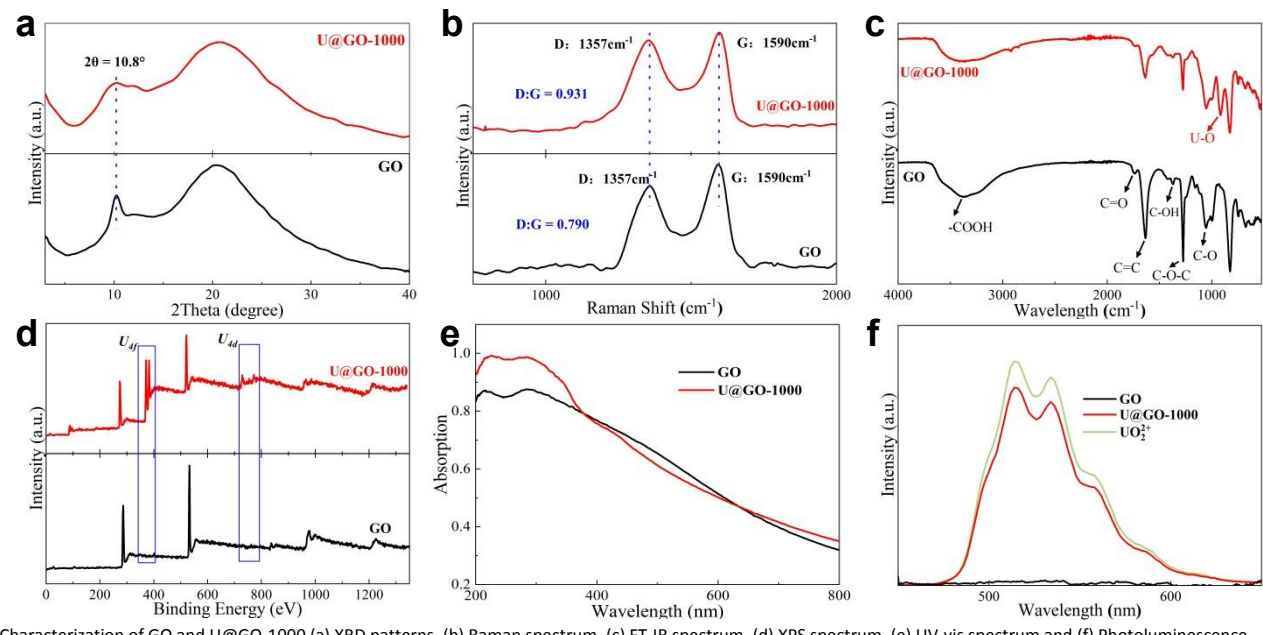


Fig. 2 Characterization of GO and U@GO-1000 (a) XRD patterns, (b) Raman spectrum, (c) FT-IR spectrum, (d) XPS spectrum, (e) UV-vis spectrum and (f) Photoluminescence spectrum.

and other spectrum characterizations (Fig. 2). The bulge observed at approximately 22° in the XRD pattern corresponds to the background signal originating from the acetate membrane substrate employed. Additionally, a characteristic peak at $2\theta = 10.8^{\circ}$ is indicative of the (002) crystal face of GO membrane, enabling calculation of layer spacing for this layered GO membrane³⁶. After the adsorption of uranyl ions, the characteristic peak exhibits a significant reduction in intensity, indicating the disruption of the original ordered stacking structure of graphene oxide (Fig. 2a). As shown in the Raman spectrum in Fig. 2b, distinct characteristic peaks of graphene oxide are observed at 1357 cm⁻¹ (D peak) and 1590 cm⁻¹ (G peak). Interestingly, while the positions of these peaks remain unchanged after uranyl ion adsorption, a notable increase in the D/G ratio is observed. This increase in the D/G ratio (from 0.790 to 0.931) suggests an increase in the proportion of defects, structural distortions, and amorphous regions within the carbon framework, which disrupts the original crystalline structure. As shown in Fig. 2c, the FT-IR spectrum reveals a new peak at approximately 900 cm⁻¹ after uranyl ion adsorption, which is assigned to the asymmetric stretching vibration of the U=O bond in uranyl ions²². The peak at around 1373 cm⁻¹ corresponds to the O-H bending vibration mode and undergoes a redshift to 1370 cm⁻¹ after graphene oxide adsorption. Furthermore, the presence of a peak at 3300 cm⁻¹ indicates involvement of alcohol hydroxyl and carboxyl groups in bending

vibrations, with degeneracy occurring upon uranyl ion $adsorption^{37}$.

To gain further insights into the role of graphene oxide and uranyl ions, XPS analysis is conducted on U@GO-1000 and GO. Firstly, upon analyzing the full spectrum in Fig. 2d, a prominent disparity between the two materials is observed: distinct U4f characteristic peak at ~400 eV and U4d characteristic peak at ~800 eV with considerable intensity. The peaks are deconvoluted based on the O1s graph (Fig.S1). The distinctive characteristics of the O1s spectrum result in its relatively broad profile, typically comprising multiple overlapping peaks that combine to form a complex spectral pattern. These peaks interfere with one another and are influenced by water and other contaminants, rendering precise analysis of the O1s spectrum exceedingly challenging. The GO spectra reveals the presence of C=O peak at 530.8 eV and C-O peak at 532.6 eV. The U@GO-1000 spectrum exhibits increased complexity, featuring two peaks corresponding to GO, as well as a distinct peak at 531.2 eV attributed to the uranyl oxygen species (O=U=O) and a U-O coordination bond at 532.3 eV³⁸. These findings further substantiate the cooperative bonding between uranyl ions and graphene oxide. Subsequently, the C1s spectrum is subjected to analysis (Fig. S2). Specifically, peaks are observed at 284.8 eV for C-C /C=C bonds, 286.7 eV for C-OH/C-O-C moieties, 287.6 eV for C=O groups, and finally at 288.8 eV for O=C-OH functionalities. The shift in peak position is not significant, but the change in peak intensity is highly noticeable, particularly

ARTICLE

with regards to the two peaks at 286.7 eV and 287.6 eV which exhibit a substantial decrease. This observation aligns with findings reported in previous literature³⁷. Fig. S3 illustrates the splitting of U4f peaks into U4f_{5/2} (395.6 eV and 392.7 eV) and U4f_{7/2} (381.9 eV and 385.0 eV). These results provide evidence that the valence state of uranyl ions remains unchanged during the interaction with GO, indicating their presence as U(VI).

To investigate the optical properties of the material, UVdiffuse reflectance and PL spectroscopy were conducted. The UV-Vis spectrum reveals absorption in both the near-ultraviolet and visible regions. Notably, the visible absorption profile is comparable to that of graphene oxide (GO), while the nearultraviolet absorption is partially attributed to the transfer of O₂p orbital electrons from uranium-oxygen bonds to nonbonding or antibonding orbitals of U in uranyl ions 39(Fig. 2e). The investigation of charge transfer transition phenomenon holds significant implications for elucidating the mechanism underlying photocatalytic oxidation⁴⁰. PL spectra are recorded at pH 5 (Fig.2f), where hydrolysis of uranyl ions occurs, resulting in the absence of a single uranyl species in the aqueous solution and leading to degeneracy in the uranyl photoluminescence spectra 41. Upon addition of GO, a reduction in fluorescence intensity is observed, providing evidence for an interaction between GO and uranyl ions that may impact their photocatalytic performance.

3.2. Photocatalytic performance

This article is licensed under a Creative Commons Attribution-NonCommercial 3.0 Unported Licence

Den Access Article. Published on 12 November 2025. Downloaded on 11/18/2025 1:42:19 AM.

The photocatalytic degradation of RhB, a non-biodegradable water contaminant, is conducted to investigate the photocatalytic performance of U@GO-1000 membrane. It is introduced into the RhB solution, for the purpose of conducting photocatalytic reactions. Upon exposure to light, it is observed that the pink color in the solution diminished while numerous bubbles emerged on the surface of the composite membrane (Fig. 3a). To evaluate the photocatalytic performance of U@GO-1000, the loading capacity of U@GO-1000 is determined using ICP-MS analysis as 2078 mg·g⁻¹ and the uranyl ion with an equal adsorption mass (1.2 mg) is both subjected to graphene oxide mass content of 0.6 mg). Subsequently, photocatalytic experiments are performed under identical conditions. The results are presented in Fig. 3b. After 4 hours of photocatalytic degradation, the GO exhibites a degradation rate of 55%, while the uranyl ion and U@GO-1000 demonstrate degradation rates of 48% and 89%, respectively. Meanwhile, no obvious selfdegradation of RhB is observed (Fig. S4).

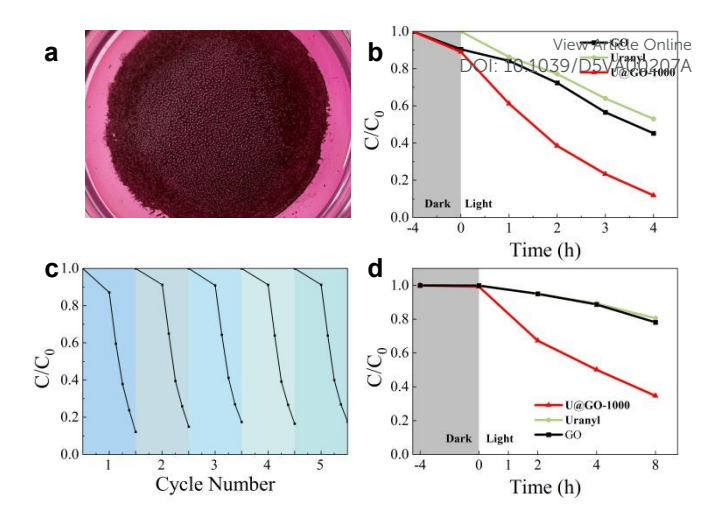


Fig. 3 Photodegradation properties with different membranes. (a) The experimental phenomenon of RhB decomposition of U@GO-1000 under light exposure. (b) Experimental results of photocatalytic degradation of RhB by GO, pure uranyl ion and U@GO-1000. (c) The results of the five-cycle RhB degradation experiment conducted on U@GO-1000. (d) Experimental results of photocatalytic degradation of TBP by GO membrane, pure uranyl ion and U@GO-1000

A pseudo-first-order reaction model is employed to fit the reaction rate constant, which is depicted in Fig. S5. The fitted k value indicates that the photocatalytic performance of U@GO-1000 surpasses that of the substrate and uranyl ion combination, thereby demonstrating an enhanced photocatalytic activity of uranyl ion after composite graphene oxide incorporation. This observation is consistent with previous findings in mesoporous silicon recombination²⁶. Recyclability of catalytic materials is a crucial parameter. Data analysis (Fig. 3d) demonstrates that the composite material retains excellent catalytic performance after five consecutive cycles, with a degradation rate exceeding 82.44%, indicating remarkable recyclability.

The application scenario of photocatalytic TBP degradation holds significant importance, thus necessitating the design and execution of experiments to validate its performance. Consequently, a photocatalytic degradation experiment targeting TBP is conducted, with the outcomes depicted in Fig. 3d. The self degradation of TBP is rarely observed under pure lighting irradiation (Fig. S6). However, upon the addition of U@GO-1000, the photocatalytic degradation rate increases to 66% within 8 h, demonstrating the capability for photocatalytic degradation of TBP of U@GO-1000. Additionally, similar bubble formation as observed during RhB degradation is also witnessed in the process of photocatalytic TBP degradation. We deduce these gaseous bubbles to be the final degradation products (CO_2) of RhB and TBP, this suggests a potential common mechanism between the degradation processes of these two distinct organic compounds: uranyl ions combine with graphene oxide and form excited states under light conditions, subsequently reacting with TBP in solution on the surface and degrading it⁴⁰. Using nitrogen gas as a carrier, the bubbles generated during the photocatalytic process were collected via the degassing method. Gas chromatography is employed to analyze the collected gases, and we detected significant CO2 peaks along with trace amounts of O2 (Fig. S7). This confirms

This article is licensed under a Creative Commons Attribution-NonCommercial 3.0 Unported Licence

Open Access Article. Published on 12 November 2025. Downloaded on 11/18/2025 1:42:19 AM

Environmental Science: Advances

that the final products of the photocatalytic degradation of the two target pollutants are CO₂, consistent with our expectations.

The spent catalysts are characterized in **Fig. S8.** The U@GO-1000 retained the membrane structure after use, and no characteristic peaks of graphene oxide are observed. The U 4f XPS spectra reveals that the uranium species dispersed on U@GO-1000 remained in the U(VI) oxidation state, which is different from the results obtained when SiO₂ is used as the substrate²⁵. This further indicates that uranyl ions are incorporated into graphene oxide through a coordination interaction and exhibit a certain bonding strength. It also explains the recyclability performance of the composite membrane.

3.3. Mechanism study

Experiments are conducted to investigate the causes of numerous bubbles observed during the photocatalytic degradation process and to explore the correlation between uranyl ion adsorption capacity and photocatalytic reaction activity. The first experiment is a conditional study, in which the concentration of uranyl ions during immersion adsorption is varied from 50 to 1000 ppm.

The results presented in Fig. S9 are obtained under identical experimental conditions and data processing methods before. The findings reveal that the photocatalytic performance of the composite exhibits a positive correlation with the concentration of uranyl ions during both immersion and adsorption stages. However, no significant variations in their properties are observed as the uranyl ion concentration changed. For instance, although there exists a two-fold difference in the impregnation stage uranyl ion concentration between U@GO-200 and U@GO-400, their photocatalytic degradation characteristics remain comparable. Moreover, when the concentration of uranyl ions during the impregnation stage is only 50 ppm, the performance is comparable to that of substrates without uranyl ions. Based on the findings from conditional and cyclic experiments, it can be inferred that most uranyl ions undergo hydrolysis and adsorption onto

the surface of graphene oxide at pH = 5 during the impregnation process, thereby preventing their bonding with graphene oxide. However, some uranyl ions form complexes with graphene oxide, where graphene oxide acts as a photoelectron acceptor in photocatalysis processes, ultimately enhancing the photocatalytic performance of uranyl ions.

In order to confirm the surface nature of the photocatalyticreaction, a two-cup experiment is devised employing a customized penetration device (Fig. 4a & S10). However, the degradation performance is reduced due to differences in effective area size between the membranes used in this experiment and those used before. Specifically, the pore size of the penetrant cup is 16mm, which represents only 11.6% of that used in other experiments (where sand core with a diameter of 47 mm is employed during extraction and filtration stages). Additionally, the amount of RhB solution has been doubled. After changing the orientation of two membranes, no decrease in RhB concentration could be observed as shown in Fig. 4b. This indicates that when the macromolecule RhB is

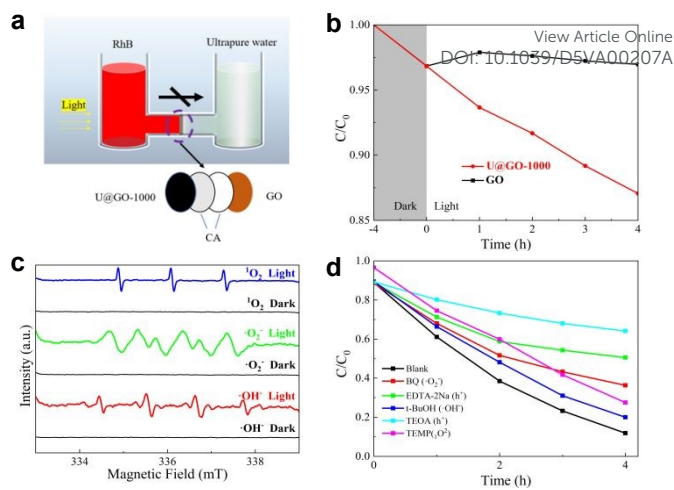


Fig. 4 (a) Schematic diagram of the two-cup experiment. (b) Results of two-cup experiment (c) ESR spectrum of U@GO-1000, the signals of hydroxyl radicals (·OH), superoxide radicals (·O₂-) and singlet oxygen (¹O₂) were measured using free radical scavengers respectively in the dark and on the light. (d) Results of scavenging experiments

physically isolated by the GO membrane, it does not undergo photodegradation. Experimental observations conducted before and after employing a GO membrane for physical isolation suggest that photodegradation necessitates direct contact between RhB and the U@GO-1000 membrane.

To clarify the photocatalytic degradation mechanism, ESR spectroscopy is performed on the U@GO-1000 (**Fig. 4c**). Distinct signals for hydroxyl radicals (\cdot OH), superoxide radicals (\cdot O₂⁻), and singlet oxygen (1 O₂) are detected under illumination, confirming their active participation in the degradation process. Notably, control experiments with GO showed no detectable radical signals, likely due to insufficient radical generation (**Fig. S11**). To identify the dominant reactive oxygen species, scavenging experiments are conducted using: benzoquinone (BQ, for superoxide radical \cdot O²⁻), EDTA-2Na and TEOA (for holes h⁺), TEMP (for singlet oxygen 1 O₂) and tert-butanol (t-BuOH, for hydroxyl radical \cdot OH-). Photodegradation efficiency decreases variably across scavenger treatments, with the most pronounced inhibition observed for hole scavengers (EDTA-2Na and TEOA), followed by weaker suppression with \cdot OH quenching (**Fig. 4d**).

To further investigate the mechanism of photocatalytic reactions, we utilized ³¹P NMR spectroscopy to monitor the intermediate products during the reaction process (**Fig. 5a**). The ³¹P NMR spectrum reveals four distinct peaks, which were assigned to MBP (1.95 ppm), DBP (0.98 ppm), phosphoric acid (0.02 ppm), and TBP (-0.12 ppm). The NMR results demonstrate

This article is licensed under a Creative Commons Attribution-NonCommercial 3.0 Unported Licence

Den Access Article. Published on 12 November 2025. Downloaded on 11/18/2025 1:42:19 AM

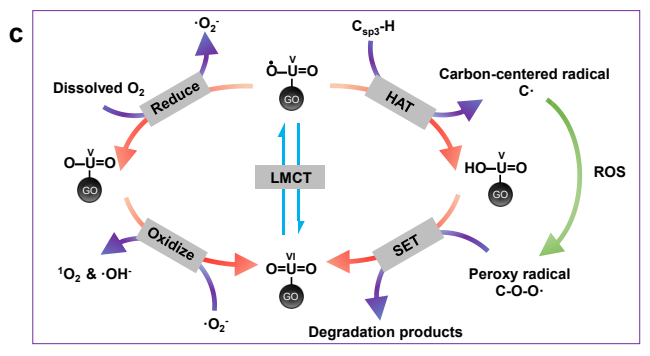


Fig. 5 (a) ³¹P NMR spectra acquired at different stages of the degradation, (b) schematic diagram of photocatalytic degradation of TBP, (c) proposed mechanism for the photocatalytic degradation of organic substances by U@GO-1000.

that during the photocatalytic degradation process, the alkyl chains of TBP are targeted and progressively decompose to form DBP, MBP, and phosphate species. These findings are consistent with well-documented observations from previous studies^{34,42}. The subsequent oxidative transformation of these alkyl chains leads to the formation of secondary degradation products, primarily lower-molecular-weight organic acids, which are ultimately mineralized into CO2 through further oxidative processes (Fig. 5b).

Combining all the previous experimental results, the propose degradation mechanism were illustrated in Fig. 5c. Under visible light irradiation, uranyl ions coordinate with oxycontaining functional groups on graphene oxide undergo LMCT processes, generating excited-state active UO₂²⁺. On one hand, the photogenerated electrons from the activated UO₂²⁺ can be separated by the graphene oxide composite, reducing dissolved oxygen in the solution to O₂.-. Subsequently, the remaining holes can further reduce the superoxide anions to ${}^{1}O_{2}$ and $\cdot OH$. These reactive oxygen species can directly participate in the degradation process. On the other hand, the activated UO22+* can attack the C(sp3)-H bonds of organic compounds via HAT, which has been extensively reported8. The reduced photocatalyst can then attack peroxide radicals through a SET process, regenerating to its initial state and completing a full catalytic cycle. Throughout this process, organic compounds are continuously attacked until they are ultimately mineralized into CO₂.

Conclusions

In conclusion, we have successfully developed a uranyl-ion functionalized graphene oxide composite membrane (U@GO-1000) via a straightforward one-step impregnation method. The composites are thoroughly characterized using analytical techniques, confirming the successful integration of uranylions into the GO and the associated structural 1937 of 5 the PARCAL modifications. The photocatalytic performance of the composites is evaluated through the degradation of RhB, demonstrating a significant enhancement compared to pure GO or uranyl ions. Moreover, the composite membrane exhibits excellent recyclability, maintaining over 80% degradation efficiency after five consecutive cycles. Notably, the U@GO-1000 demonstrates high efficiency in the photocatalytic degradation of radioactive TBP, highlighting its substantial potential for application in treating radioactive TBP waste generated in the Purex spent nuclear fuel reprocessing cycle. A mechanistic analysis reveals that the specific interaction between uranyl ions and graphene oxide facilitates the generation of highly oxidizing photogenerated holes and a substantial quantity of reactive oxygen species upon illumination. Besides, the excited UO₂²⁺ directly attacks the C-H bonds of organic via a hydrogen atom transfer mechanism. This dual-action process continuously dismantles TBP until it is fully converted into harmless small molecules like carbon dioxide (CO₂), achieving complete mineralization. This study offers a new perspective on the utilization of depleted uranium and introduces a novel material and methodology for the photocatalytic degradation of TBP, a challenging organic pollutant in radioactive wastewater. The findings underscore the potential of U@GO-1000 as an efficient and sustainable solution for addressing radioactive wastewater treatment challenges.

Author contributions

Conceptualization, Jiahui Ying, Liqin Huang, Shanshan Yu, Shuang Liu; methodology, Jiahui Ying, Liqin Huang, Shanshan Yu, Shuang Liu; supervision, Zhe Wang, Jing Chen, Yuexiang Lu; writing-original draft, Jiahui Ying; writing-review and editing, Zhe Wang, Jing Chen, Yuexiang Lu. All authors have read and agreed to the published version of the manuscript.

Data availability

The data results are all presented in the paper and can be used if cited.

Conflicts of interest

There are no conflicts to declare.

Acknowledgements

This work was financially supported by the National Natural Science Foundation of China (Grant No. 22376059, 22422606, U2341289).

Notes and references

ARTICLE Environmental Science: Advances

- 1 M. R. Duff, Jr. and C. V. Kumar, Site-selective photocleavage of proteins by uranyl ions, *Angew Chem Int Ed Engl*, 2005, 45, 137-139.
- J. G. West, T. A. Bedell and E. J. Sorensen, The Uranyl Cation as a Visible-Light Photocatalyst for C(sp(3))-H Fluorination, Angew Chem Int Ed Engl, 2016, 55, 8923-8927.
- 3 Q. Zhang, B. Jin, R. Peng, X. Wang, Z. Shi, Q. Liu, S. Lei and H. Liang, Investigation on the Synthesis and Photocatalytic Property of Uranyl Complexes of the β-Diketonates Biscatecholamide Ligand, *Int. J. Photoenergy*, 2017, 2017, 1-12.
- 4 K. Takao and S. Tsushima, The oxidation of borohydrides by photoexcited [UO(2)(CO(3))(3)](4-), *Dalton Trans.*, 2018, 47, 5149-5152.
- 5 Y. Zhou, D. Hu, D. Li and X. Jiang, Uranyl-Photocatalyzed Hydrolysis of Diaryl Ethers at Ambient Environment for the Directional Degradation of 4-O-5 Lignin, *JACS Au*, 2021, 1, 1141-1146.
- 6 J. Meng, Y. Zhou, D. Li and X. Jiang, Degradation of plastic wastes to commercial chemicals and monomers under visible light, Sci. Bull., 2023, 68, 1522-1530.
- 7 Y. Meng, D. Liu, Q. Lan, Z. Xie, F. Niu, X. Zhang and Y. Yang, Synthesis, structure, and photocatalytic properties of a twodimensional uranyl organic framework, Z. Kristallogr. Cryst. Mater., 2023, 238, 65-71.
- 8 G. Che, W. Yang, J. Luo, M. Li, X. Li and Q. Pan, Efficient adsorption and photocatalysis over a photorenewable uranylorganic framework for removal of diquat herbicide, *Sep. Purif. Technol.*, 2024, 334.
- 9 X. Gong, Q. Zhao and C. Zhu, Visible-Light-Initiated Uranyl-Catalyzed Hydrosilylation and Hydrosulfonylation of Alkenes and Alkynes, Adv. Synth. Catal., 2024, 367.
- 10 X. Wang, J. Li, X. Wei, J. Song, J. Xie, Z. Li, M. Yuan, L. Jiang, Y. Wang, C. Liang and W. Liu, Photocatalytic Hydrogen Peroxide Production by a Mixed Ligand-Functionalized Uranyl–Organic Framework, ACS Omega, 2024, 9, 33671-33678.
- 11 X. Zhao, L. Bai, J. Li and X. Jiang, Photouranium-Catalyzed C–F Activation Hydroxylation via Water Splitting, *J. Am. Chem. Soc.*, 2024, 11173-11180.
- 12 B. w. Hu, W. Jin, Z. w. Huang, Z. h. Zhou, K. q. Hu, L. y. Yuan, H. b. He, W. q. Shi and L. Mei, Integrating Uranyl Complexes into Porous Organic Cages for Enhanced Photocatalytic Oxidation of A Mustard-Gas Simulant, Eur. J. Inorg. Chem., 2025, 28.
- 13 Y. X. Liu, L. Jia, Y. R. Li, P. W. Cai, M. R. Ou, C. Sun and S. T. Zheng, Bridging Uranium Uptake and PET Plastics Degradation Within an All-Inorganic Polyoxoniobate Framework, *Adv. Funct. Mater.*, 2025, e16939.
- 14 S.-B. Tang, S.-Y. Zhang, Y.-X. Jiang, Z.-X. Wang, K. Li, Y.-Y. Luo, B. Long and J. Su, Visible-Light-Induced Photocatalytic Degradation of Polyvinyl Chloride under Normal Temperature and Pressure via Uranyl Photocatalyst, *Ind. Eng. Chem. Res.*, 2025, 64, 7661-7669.
- 15 L.-Y. Wang, G. Che, Y.-R. Gong, W.-T. Yang, Y. Lin, J.-R. Liu, S.-Y. Chen, M.-D. Xiao, X.-D. Tian and Z.-M. Su, Temperature-driven growth of uranyl-organic frameworks for efficient photocatalytic CO2 reduction, *Inorg. Chem. Front.*, 2025, 12, 3262-3269.
- 16 D. R. Hartline and K. Meyer, From Chemical Curiosities and Trophy Molecules to Uranium-Based Catalysis: Developments for Uranium Catalysis as a New Facet in Molecular Uranium Chemistry, *JACS Au*, 2021, 1, 698-709.
- 17 N. Behera and S. Sethi, Unprecedented Catalytic Behavior of Uranyl(VI) Compounds in Chemical Reactions, *Eur. J. Inorg. Chem.*, 2020, 2021, 95-111.
- 18 A. R. Fox, S. C. Bart, K. Meyer and C. C. Cummins, Towards uranium catalysts, *Nature*, 2008, 455, 341-349.

- 19 X. Bai, L. Wang, R. Zong, Y. Lv, Y. Sun and Y. Zhu, Refronted name enhancement of ZnO photocatalyst wia synesgio 50年 surface oxygen defect and graphene hybridization, Langmuir, 2013, 29, 3097-3105.
- 20 Y. Liu, Z. Yu, Y. Peng, L. Shao, X. Li and H. Zeng, A novel photocatalytic self-cleaning TiO2 nanorods inserted graphene oxide-based nanofiltration membrane, *Chem. Phys. Lett.*, 2020, 749.
- 21 T. Peik-See, A. Pandikumar, L. H. Ngee, H. N. Ming and C. C. Hua, Magnetically separable reduced graphene oxide/iron oxide nanocomposite materials for environmental remediation, *Catal. Sci. Technol.*, 2014, 4, 4396-4405.
- 22 K. Vidya, S. Dapurkar, P. Selvam, S. Badamali and N. Gupta, The entrapment of UO22+ in mesoporous MCM-41 and MCM-48 molecular sieves, *Microporous Mesoporous Mater.*, 2001, 50, 173-179.
- 23 S. L. Suib and K. A. Carrado, Uranyl clay photocatalysts, *Inorg. Chem.*, 1985, 24, 863-867.
- 24 J. A. Nieweg, K. Lemma, B. G. Trewyn, V. S.-Y. Lin and A. Bakac, Mesoporous silica-supported uranyl: synthesis and photoreactivity, *Inorg. Chem.*, 2005, 44, 5641-5648.
- 25 D. S. Selishchev, T. N. Filippov, M. N. Lyulyukin and D. V. Kozlov, Uranyl-modified TiO2 for complete photocatalytic oxidation of volatile organic compounds under UV and visible light, Chem. Eng. J., 2019, 370, 1440-1449.
- 26 L. Zheng, N. Zhao, L. Zhang, S. Liu, Z. Wang, X. Wang and Y. Lu, Treating waste with waste: Facile preparation of uranyl based photocatalyst for efficient degradation of organic dyes, J. Environ. Chem. Eng., 2024, 12.
- 27 T. F. Williams, R. W. Wilkinson and T. Rigg, Radiolysis of Tri-nbutyl Phosphate, *Nature*, 1957, 179, 540-540.
- 28 J. G. Burr, The Radiolysis of Tributyl Phosphate, *Radiat. Res.*, 1958, 8, 214-221.
- 29 X. Ouyang, B. Fan, H. Yang and R. Qing, Research on Air Content Estimation of Tributyl Phosphate Hydraulic Fluids: A Novel Approach Based on the Vacuum Method, *J. Dyn. Syst. Meas. Contr.*, 2014, 136.
- 30 T. P. Valsala, M. S. Sonavane, S. G. Kore, N. L. Sonar, V. De, Y. Raghavendra, S. Chattopadyaya, U. Dani, Y. Kulkarni and R. D. Changrani, Treatment of low level radioactive liquid waste containing appreciable concentration of TBP degraded products, *J. Hazard. Mater.*, 2011, 196, 22-28.
- 31 H. Aly, Wet-oxidation of spent organic waste tributyl phosphate/diluents, *J. Radioanal. Nucl. Chem.*, 2001, 249, 643-647.
- 32 S. S. Rangu, B. Muralidharan, S. C. Tripathi and S. K. Apte, Tributyl phosphate biodegradation to butanol and phosphate and utilization by a novel bacterial isolate, Sphingobium sp. strain RSMS, *Appl. Microbiol. Biotechnol.*, 2014, 98, 2289-2296.
- 33 M. J. Watts and K. G. Linden, Photooxidation and subsequent biodegradability of recalcitrant tri-alkyl phosphates TCEP and TBP in water, *Water Res.*, 2008, 42, 4949-4954.
- 34 E. Drinks, C. Lepeytre, C. Lorentz, M. Dunand, S. Mangematin, F. Dappozze and C. Guillard, UV-a photocatalytic degradation of the radionuclide complexants tributylphosphate and dibutylphosphate, *Chem. Eng. J.*, 2018, 352, 143-150.
- 35 Z. Wang, L. Huang, X. Dong, T. Wu, Q. Qing, J. Chen, Y. Lu and C. Xu, Ion sieving in graphene oxide membrane enables efficient actinides/lanthanides separation, *Nat. Commun.*, 2023, 14, 261.
- 36 D. Zhao, L. Chen, M. Xu, S. Feng, Y. Ding, M. Wakeel, N. S. Alharbi and C. Chen, Amino Siloxane Oligomer Modified Graphene Oxide Composite for the Efficient Capture of U(VI) and Eu(III) from Aqueous Solution, ACS Sustainable Chem. Eng., 2017, 5, 10290-10297.
- 37 S. Song, K. Wang, Y. Zhang, Y. Wang, C. Zhang, X. Wang, R. Zhang, J. Chen, T. Wen and X. Wang, Self-assembly of

nvironmental Science: Advances Accepted Manuscript

View Article Online

DOI: 10.1039/D5VA00207A

Journal Name ARTICLE

graphene oxide/PEDOT:PSS nanocomposite as a novel adsorbent for uranium immobilization from wastewater, *Environ. Pollut.*, 2019, 250, 196-205.

- 38 M. Schindler, F. C. Hawthorne, M. S. Freund and P. C. Burns, XPS spectra of uranyl minerals and synthetic uranyl compounds. II: The O 1s spectrum, Geochim. *Cosmochim. Acta*, 2009, 73, 2488-2509.
- 39 V. A. Volkovich, T. R. Griffiths, D. J. Fray and R. C. Thied, The electronic spectra of alkali metal uranates and band assignments: an analysis of their diffuse reflectance spectra, *Phys. Chem. Chem. Phys.*, 2001, 3, 5182-5191.
- 40 Z. T. Yu, Z. L. Liao, Y. S. Jiang, G. H. Li and J. S. Chen, Water-insoluble Ag-U-organic assemblies with photocatalytic activity, *Chemistry*, 2005, 11, 2642-2650.
- 41 M. E. D. G. Azenha, H. D. Burrows, S. J. Formosinho, M. G. M. Miguel, A. P. Daramanyan and I. V. Khudyakov, On the uranyl ion luminescence in aqueous solutions, *J. Lumin.*, 1991, 48-49, 522-526.
- 42 T. D'Halluin, C. Lepeytre, A. Leydier and C. Julcour, Degradation mechanism of tributyl phosphate by UV/H(2)O(2) treatment and parameters optimization towards the design of a pilot reactor, *Environ. Technol.*, 2021, 42, 4247-4259.

View Article Online DOI: 10.1039/D5VA00207A

Open Access Article. Published on 12 November 2025. Downloaded on 11/18/2025 1:42:19 AM.

This article is licensed under a Creative Commons Attribution-NonCommercial 3.0 Unported Licence.

Data availability statement (DAS)

- Data for this article, including figures and tables are available at URLhttps://doi.org/DOI.
- 2. The data supporting this article have been included as part of the Supplementary Information.